Hearing Research 405 (2021) 108234

Contents lists available at ScienceDirect

Hearing Research

journal homepage: www.elsevier.com/locate/heares

Research Paper

Nonlinearity of intracochlear motion and local cochlear microphonic: Comparison between guinea pig and gerbil

Elika Fallah[a], C. Elliott Strimbu[b], Elizabeth S. Olson[a,b,*]

[a] Department of Biomedical Engineering, Columbia University, New York City, NY, United States
[b] Department of Otolaryngology-Head and Neck Surgery, Columbia University, New York City, NY, United States

ARTICLE INFO

Article history:
Received 20 November 2020
Revised 8 March 2021
Accepted 26 March 2021
Available online 15 April 2021

ABSTRACT

Studying the *in-vivo* mechanical and electrophysiological cochlear responses in several species helps us to have a comprehensive view of the sensitivity and frequency selectivity of the cochlea. Different species might use different mechanisms to achieve the sharp frequency-place map. The outer hair cells (OHC) play an important role in mediating frequency tuning. In the present work, we measured the OHC-generated local cochlear microphonic (LCM) and the motion of different layers in the organ of Corti using optical coherence tomography (OCT) in the first turn of the cochlea in guinea pig. In the best frequency (BF) band, our observations were similar to our previous measurements in gerbil: a nonlinear peak in LCM responses and in the basilar membrane (BM) and OHC-region displacements, and higher motion in the OHC region than the BM. Sub-BF the responses in the two species were different. In both species the sub-BF displacement of the BM was linear and LCM was nonlinear. Sub-BF in the OHC-region, nonlinearity was only observed in a subset of healthy guinea pig cochleae while in gerbil, robust nonlinearity was observed in all healthy cochleae. The differences suggest that gerbils and guinea pigs employ different mechanisms for filtering sub-BF OHC activity from BM responses. However, it cannot be ruled out that the differences are due to technical measurement differences across the species.

1. Introduction

The evolution of the mammalian ear resulted in both general and species-specific features. The penetration of bone into the soft tissues in the cochlea, the formation of the cochlea's coiled shape and the profound series of changes in the micro and macro structures of the cochlear partition (e.g. the arrangement of two types of sensory cells, mechanical developments of the basilar and tectorial membranes), all together, paved the way to a hearing organ able to process higher frequencies (Vater and Kossl, 2011; Manley, 2010, 2018). To adapt to specific habitats, mammals developed different cochlear specializations. Some became maximally sensitive to specific frequency ranges. For example, the audiograms of bats and dolphins are sharply tuned to the frequencies that they use for echolocation, between 20 and 100 kHz. To be able to perceive such high frequencies, the mustached bat's cochlea has exceptionally large basal fluid chamber volumes, and a thickened tectorial membrane (TM) in the base relative to the apex (Henson, 1973; Hensen et al., 1977; Thorne et al., 1999). Humans and elephants can hear frequencies as low as 20 Hz, but their upper limit is restricted to ~ 20 kHz. Gerbils have an unusual basilar membrane (BM) shape compared to guinea pigs and human and a wider hearing range (~ 100 Hz–60 kHz) compared to most other rodents (Fay, 1989; Kapuria et al., 2017). Guinea pigs also have a wide hearing range (~54 Hz–50 kHz Fay, 1989) but in the evolutionary path, gerbils and guinea pigs are not specifically related. Gerbils belong to the murid classification in the rodent family; guinea pigs are a non-murid species (Reyes et al., 2000; Vater and Kossl, 2011). We compared cochlear responses in these two species in order to shed light on strategies employed for sharp frequency tuning.

The outer hair cells (OHCs) are powerful mechano-sensory cells in the cochlea. The *mechano-electric transduction* (MET) channels on the stereocilia bundles of the OHC control the current through the OHC and thus the OHC voltage. When the intracellular voltage changes, the OHC exerts force on the organ of Corti complex (OCC = organ of Corti (OC) + its surrounding membranes, BM and TM). At low to moderate sound pressure levels (SPL), OHC electromotility creates a positive feedback to increase the amplitude of OCC motion - a phenomenon termed cochlear amplification. This feedback is compressively nonlinear; the saturation of the MET channels on the OHC stereocilia bundle is considered to be the

* Corresponding author at: 630 West 168th Street, New York, NY 10032 United States.
E-mail address: eao2004@columbia.edu (E.S. Olson).

https://doi.org/10.1016/j.heares.2021.108234
0378-5955/

dominant source of nonlinearity in cochlear amplification (Santos-Sacchi, 1993; Geisler et al., 1990). Before Optical Coherence Tomography (OCT) emerged in the field of cochlear mechanics, we and others have mainly studied the amplification measurable at the BM (Rhode, 1971, 2007; De Boer and Nuttall, 1997, 2000; Dong and Olson, 2013, 2016; Fridberger et al., 2004; Eze and Olson, 2011; Ren, 2002; Narayan et al., 1998). Observing the BM motion frequency responses measured at a single location, it is established that the BM amplification peaks in a limited bandwidth, termed the best frequency (BF) band. The frequency responses below the peak are referred to as "sub-BF" responses. Since we and others started using OCT, we have been able to image and simultaneously measure the displacements of the BM and the layers beyond the BM along the axis of the OCT beam.

In a previous study we measured the displacements of the BM and the OHC region in gerbil (Fallah et al., 2019*)*. We also measured the local cochlear microphonic (LCM) at the same longitudinal location. The LCM – a measure of local OHC current, and indirectly OHC voltage – represents the expected drive to OHC electromotility. Measuring it along with motion informs our understanding of cochlear amplification. In gerbil we observed a similar nonlinear character in the LCM and the OHC-region motions: sharp tuning and nonlinearity in the BF band and a nonlinearity in the sub-BF band that was not observed in the BM motion. We observed sub-BF nonlinearity in the OHC-region basal motions in all healthy gerbil cochleae. Given that OHC electromotility is wideband (Frank et al., 1999; Rabbitt, 2020*),* and the LCM, representing OHC current, is nonlinear, the observation of sub-BF nonlinearity in the OHC region was not a surprise. However, by boosting the response at frequencies off the BF, the presence of the sub-BF nonlinearity is detrimental to the frequency resolution. Related to the difference between sub-BF and BF bands, in measurements in gerbil, Dong and Olson (2013) observed a phase shift in the LCM at a frequency about 0.7 x BF, which is associated with the onset of BM amplification. In the paper's analysis, at frequencies above/below the phase shift, OHC electromotility would/would-not be phased correctly to provide power amplification to the BM motion. The BM is thought to be the main structural support for the cochlear traveling wave, which is responsible for transporting sound energy down the cochlea (Olson, 2020). The phase shift might be produced by the mechanics of the stereocilia and the TM (Nankali et al., 2020).

Guinea pig has long been an auditory model used in studies of cochlear mechanics (Cooper and Rhode, 1992; Sellick et al., 1983; Nuttall et al., 2018). Recently, pioneering measurements of intracochlear motions were made using time-domain OCT (Chen et al., 2011), in which the vibrations of locations within the OCC are measured sequentially. Here we use spectral-domain OCT, in which the vibrations of different locations within the OCC are measured simultaneously. We report on the tuning and degree of nonlinearity in intracochlear motion and LCM in the cochlear base. We describe how BM responses differ from OHC-region responses, and compare gerbil and guinea pig responses in BF and sub-BF bands.

2. Materials and methods

2.1. Animal preparation

Methods are described for guinea pigs. The gerbil data derived from previously published studies (Fallah et al., 2019; Strimbu et al., 2020). The methodology in gerbils and guinea pigs is very similar with the exceptions of anesthesia (isoflurane: guinea pig, pentobarbital: gerbil) and access for motion measurements (cochleostomy: guinea pig, RW opening: gerbil).

Forty juvenile guinea pigs between 180 and 300 g of both sex were used in this study and results from twelve are reported. Several animals were used to develop the approach. In other non-reported experiments, the cochleostomy caused damage, the spontaneous contraction of the tensor tympani motion disrupted the imaging, or the animals died prematurely. The reported data were chosen based on signal-to-noise ratio and in the case of LCM, response size, since it declines with distance from the BM. The experiments were approved by the Institutional Animal Care and Use Committee of Columbia University. Cochlear measurements were conducted while the animals were deeply anesthetized with isoflurane inhalant. A regulated heating blanket maintained the body temperature at ~38 °C. The left bulla was opened with forceps using a posterior approach so that the round window (RW) and the first turn of the cochlea were accessible (Fig. 1A). In order to get access to lower frequency ranges (BF ~ 23 kHz), a small hole (diameter ~200–300 μm for motion measurements and less than 200 μm for LCM) was hand-drilled in the basal turn of the cochlear capsule, ~0.4 mm apical of the RW. The BFs of the measurements in gerbil were slightly larger, on average 27 kHz. Acoustic stimuli were generated by a Tucker Davis Technologies system and were presented closed-field to the ear canal (EC) by a Radio Shack dynamic speaker. A Sokolich ultrasonic microphone (WGS & Associates, Newport Beach, CA) was coupled to the speaker tube for sound calibration just inside the EC.

To ensure that the cochlea was in a healthy state, in three animals of the twelve (GP 6, 21 & 23) compound action potentials (CAPs) were measured with an electrode at the round window before and after the cochleostomy (Fig. 1B). In the other nine reported experiments, for the sake of time, instead of CAP, distortion product otoacoustic emissions (DPOAEs) were measured in response to a two-tone stimulus with fixed frequency ratio ($f_2/f_1 = 1.25$) and equal stimulus levels (60, 70 and 80 dB SPL). In Fig. 1D the average difference in DPOAEs at a frequency of $2f_1$-f_2 in response to 60 dB SPL stimuli before and after cochleostomy are shown. The DPOAEs in response to all three SPLs are shown for one animal in Fig. 1C. These twelve cochleae (eight cochleae for the motion measurements and eight cochleae for the LCM experiments, with four cochleae used for both motion and LCM measurements) were in good condition following the cochleostomy. In the four cochleae where both motion and LCM responses were measured (GP 26, 29, 34 & 35), LCM measurements were made before the OCT motion and the DPOAEs were stable between the two sets of measurements.

2.2. Motion measurements

A ThorLabs Telesto III spectral domain optical coherence tomography (SD-OCT) system was used to simultaneously measure the displacements of different layers in the OCC through a hole in the basal turn of the cochlea. A Thorlabs LSM03 objective lens with lateral resolution of 13 μm was used. The axial resolution (spacing between adjacent axial pixels) was ~ 2.7 μm. A two-dimensional scan, termed a *B*-scan, was obtained for a cross-sectional view of the basal OCC. A one-dimensional depth profile, termed an axial-scan (*A*-scan), was taken at one radial location within the *B*-scan, and was typically selected to include the OHC region (Fig. 2). Our SD-OCT system has been customized by our group such that a series of time-locked *A*-scans, termed an *M*-scan, can be acquired and processed. In the *M*-scan, the time-dependent phase of each pixel in the *A*-scan corresponds to the motion of the OCC at that location (Lin et al., 2017, 2018). After taking an *M*-scan, the radial location of the *A*-scan was changed and additional *M*-scans were taken. Motion responses are shown in OHC-region and BM-region pairs, with data collected simultaneously from the same *M*-scan. In several experiments motion measurements were made in the same cochlea before or after the LCM measurements. Depending on the direction of the OCT beam, and the radial location where

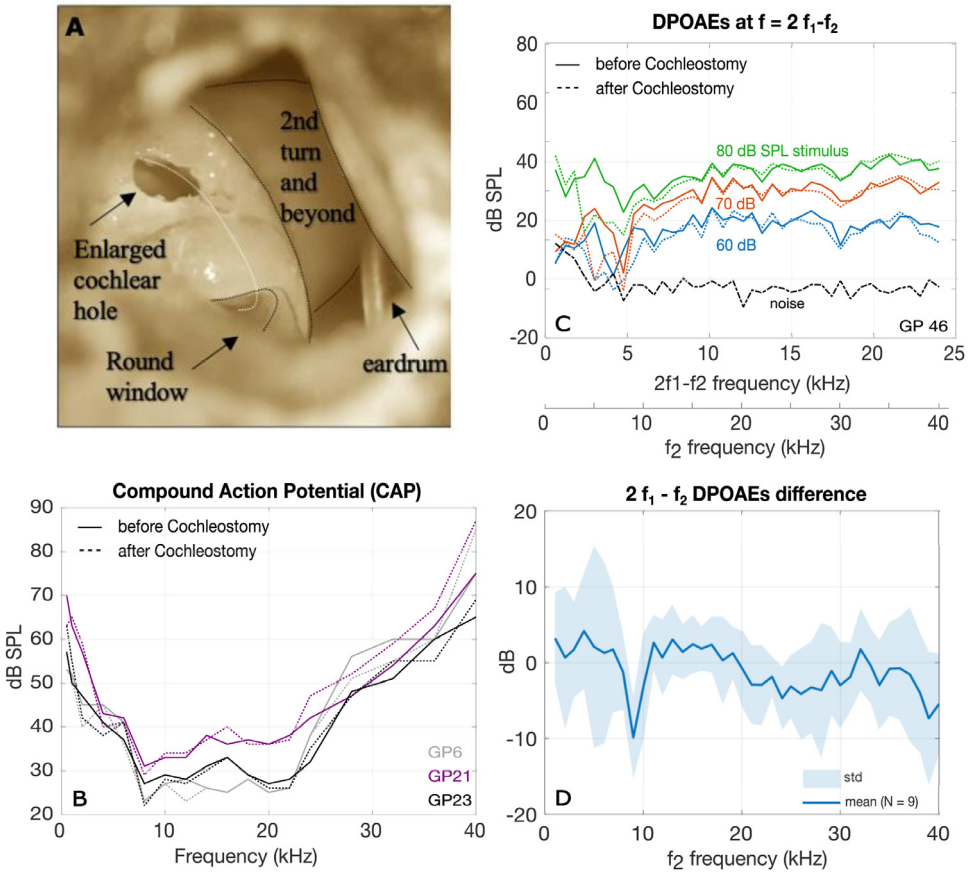

Fig. 1. (A) Experimental view of the base of the guinea pig cochlea through an opening in the bulla. The round window (RW) and part of the cone of the cochlea (2nd turn and beyond) are in view. A hand-drilled hole (enlarged for this photo after the measurements were made) ~ 0.4 mm apical of the RW is seen. The white dotted line indicates the path of the BM inside the cochlea. (B) Compound action potential (CAP) thresholds before (solid lines) and after the cochleostomy (dotted lines) for three animals. (C) Distortion product otoacoustic emissions (DPOAEs) at frequency of $2f_1 - f_2$ in response to 60, 70 and 80 dB SPL two-tone stimuli ($f_2/f_1 = 1.25$), before (solid lines) and after the cochleostomy (dotted lines) for one animal (GP 46). (D) Group data from nine animals of the difference in DPOAEs before and after the cochleostomy. The primary level was 60 dB SPL. From 15 to 35 kHz the changes in DPOAE level were on average less than 4 dB, and were deemed acceptable.

the beam was aimed, the reflectivity of each pixel in the *A*-scan varied and that affected the signal-to-noise ratio (SNR) of the motion responses. The noise floor in the best OCT recordings was ~ 50 pm. The displacement responses reported here were above a SNR threshold, such that their amplitudes were at least three standard deviations above the mean noise floor measured within ten neighboring points in the frequency domain. The sound stimulus sent to the EC consisted of multi-tones (40 or 60 Zwuis tone complexes), 10–80 dB SPL per tone in 10 dB SPL steps (SPL is defined as dB re 20 μPa). The characteristics of the multi-tone stimuli were previously described (Fallah et al., 2019; Versteegh and van der Heijden, 2012). Each stimulus run was ~5 s in duration. The sampling rate for the OCT recordings was ~100 kHz (the OCT system is limited to operate below 200 kHz) and recorded data were not averaged. Image and data processing were performed using custom MATLAB (MathWorks R2016b & R2017b) scripts.

Due to technical-amplifier and experimenter-choice reasons, the number of tones in the multi-tone stimulus was either 40 or 60 tones. The gerbil LCM multi-tone stimuli were composed of 40 tones and the gerbil OCT multi-tone stimuli were 60 tones. For the guinea pig, almost all data (LCM and OCT) were taken with 60 tones, and the few runs with 40 tones did not show systematic differences in gain factor. The overall stimulus level increase of 60 compared to 40 tones would be $20\log\sqrt{60/40} = 1.76\,dB$, which is small compared to the overall stimulus range, and was not expected to influence the results. No influence was apparent.

2.3. Measurement of the angles formed between intracochlear structures

Although we cannot clearly discern the inner and outer hair cells in the OCT B-scans, by comparing to known anatomy, we can detect important features, identified in Fig. 2. We can find the BM angle relative to the horizontal line (η), and identify the cross section of the tunnel of Corti (ToC). The ToC is a fluid gap that does not reflect light; thus, it is seen as a dark space in the B-scan (Fig. 2A). We can estimate the approximate location of the OHCs and IHCs. Based on the study by Fernández (1952) in guinea pig, at distances between 0 and 3.5 mm from the base, the angle formed between the OHCs and the BM (β) and the angle between OHCs and IHCs (γ) were estimated to be β ~ 40°–50° and γ ~ 60°–70°. Fernandez reported that a constant angle of α~65° formed by the axis of the BM and the IHCs is present from the base to the apex. The internal angles measured in the first turn of the guinea pig hemicochlea (~14 mm from the apex) were reported to be α~ 66° ± 3.75° ($N = 8$) and β~ 52° ± 2.17° ($N = 8$) (Teudt and Richter, 2007). Our cochlear responses were tuned to BF ~22–24 kHz – which corresponds to a distance of ~ 1.5–1.7 mm from the base (~ 16.5–16.3 mm from the apex) based on the frequency-location map in guinea pig (Greenwood, 1990). Consistent with *Fernández* and *Teudt and Richter*, we measured α~65° and γ~75° in our *B*-scans (Fig. 2B). Therefore, the angle formed between the OHCs and the BM (β) would be ~ 40°. The BM angle relative to the horizontal line (η), and thus, the angle between the OCT beam and the axis

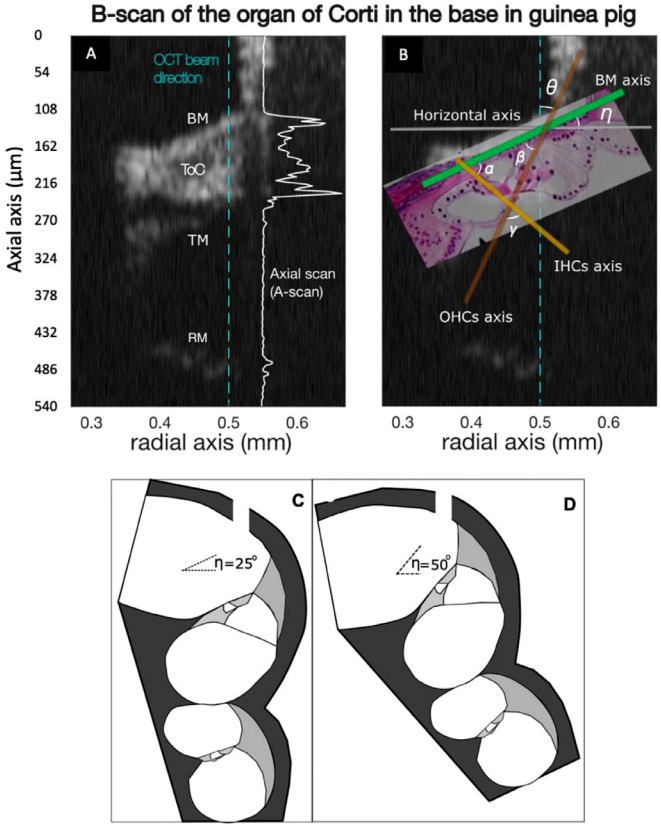

Fig. 2. (A) B-scan of the organ of Corti through a hand-drilled hole in the base of the cochlea in guinea pig (BF~22.6 kHz). Basilar membrane (BM), Tunnel of Corti (ToC), Tectorial membrane (TM) and Reisner's membrane (RM) are labeled. The OCT beam (vertical cyan dashed line) was directed from the top. The vertical (axial) resolution was ~2.7 µm per pixel and the axis is labeled in µm units. The white line indicates the magnitude of the *A*-scan. Motion was measured at local maxima in the *A*-scan, where SNR is relatively high. (B) A histological image of the OCC of guinea pig in the base (Raufer et al., 2019) was placed on top of the *B*-scan in panel (A). α = the angle between the BM and inner hair cells (IHCs) (yellow line is the axis of IHCs). β = the angle between the BM and OHCs (brown line is the axis of the OHCs). γ = the angle between OHCs and IHCs. θ = the angle between the OCT beam and the OHCs. η = the BM angle relative to the horizontal line. (C & D) Two schematics of the cross-section of the cochlea showing two different BM angles relative to the horizontal line. η depended on the precise position of the cochleostomy and varied somewhat between preparations.

of the OHCs (θ) varied in different experiments, and differences based on this angle are explored.

2.4. Local cochlear microphonic (LCM) measurements

LCM measurements were performed in eight guinea pigs. A tungsten electrode, insulated to its tip (FHC, Bowdoin ME) was inserted through a hand-drilled hole in scala tympani and positioned close to the BM. The reference electrode was a silver wire placed in the neck muscle. Multi-tone stimuli similar to those used in the motion measurements were sent to the EC. In addition to the multi-tone stimuli, single-tone acoustic stimuli (10 to 90 dB SPL in 10 dB steps, ~ 1–40 kHz in 500 Hz steps) were also used. A higher sampling rate (~200 kHz) compared to the OCT measurements (~100 kHz) was used for the LCM measurements to allow us to evaluate harmonics (not reported here).

3. Results

The results section starts with motion responses in guinea pig - these are the substantial new data of this paper. Displacements were measured at 5–17 different radial locations (*A*-scans) in each preparation, and 3–5 angles were also explored. A table of motion metrics is generated. Next motion responses in gerbil are shown and tabulated. The next section introduces the comparison between the two species: The phenomenon of hyper-compression is compared with examples in the two species. Then LCM results from the two species and a table of LCM metrics are presented. The results section ends with grouped data where responses from the two species are compared in a bar-graph format.

3.1. Motion responses in guinea pig

The BM and OHC-region displacements in response to multi-tone stimuli from two guinea pigs are shown in Figs. 3 and 4 (results from two additional animals are in supplemental material, Figs. S1 and S2). In both regions, displacements were largest at the BF, slightly over 20 kHz, where they grew nonlinearly with stimulus level. The phase of both the BM and OHC-region motion responses accumulated through several cycles, indicating the cochlear traveling wave delay. The displacements were substantially greater in the OHC region than at the BM in all eight cochleae (gains in nm/Pa are in Table 1). The BF motion gain factor (GF_{BF}), defined as the ratio of the 40 dB SPL motion gain to the 80 dB SPL motion gain, calculated at the BF found at 40 dB SPL is also in Table 1. The 40–80 dB range was used to provide consistency across experiments.

In the sub-BF band, the BM motion grew essentially linearly (Figs. 3 and 4). In the OHC region, from eight OCT experiments, only four showed sub-BF motion nonlinearity (Fig. 4). In those four the sub-BF motion gain factor, defined as the ratio of the 40 dB SPL motion gain to the 80 dB SPL motion gain at a frequency between 9 and 11 kHz (GF_{sub}), was much less than in the BF region (Table 1).

$Q_{10\ dB}$, defined as the BF divided by the frequency bandwidth 10 dB below the peak, at 40 dB SPL, was calculated for the BM and the OHC region. The $Q_{10\ dB}$ values spanned from 2.8 to 5.1 and were similar in the two regions; a statistical comparison is in Fig. 9.

Post-mortem motion measurements were made in two animals, with results from one shown in dashed lines in Fig. 3B. Both the BM and the OHC-region BF motions dropped and became linear post-mortem. In the OHC region the sub-BF motions *in-vivo* were larger than the sub-BF motions post-mortem. It is notable that this post-mortem reduction was observed even though sub-BF nonlinearity was not observed. On the BM, the sub-BF motions were similar and linear pre and post-mortem. Post-mortem measurements were not made in all animals, in part because they were not always possible due to reduced SNR post-mortem.

Considerations of angle: The BM angle relative to the horizontal line (η) and consequently, the angle between the OCT beam and the axis of the OHCs (θ) varied between preparations. Considering the internal cochlear angles as α=65°, β = 40° and γ= 75°, when the BM angle relative to the horizontal line (η) is greater than 35°, the angle formed between the axis of the OHCs and the OCT beam (θ) will be less than ~15°. We hypothesized that sub-BF nonlinearity would be more detectable when the OCT was more aligned with the OHCs. However, robust angle-dependent variations in the motion, in particular with respect to the detection of sub-BF nonlinearity in the OHC regions, were not observed (Table 1).

Considerations of radial location in motion responses: In Fig. 5, the intracochlear motion responses to multi-tone stimuli are shown at two different radial locations in two guinea pig cochleae. The blue colored *A*-scans were directed to a radial location 20 µm (in GP 46) and 40 µm (in GP 32) lateral (towards the spiral ligament) relative to the red colored *A*-scans. In GP 46, the BM motion responses were linear in the sub-BF band and showed a nonlinear peak in the BF band, with a slightly larger peak at location 3 compared to

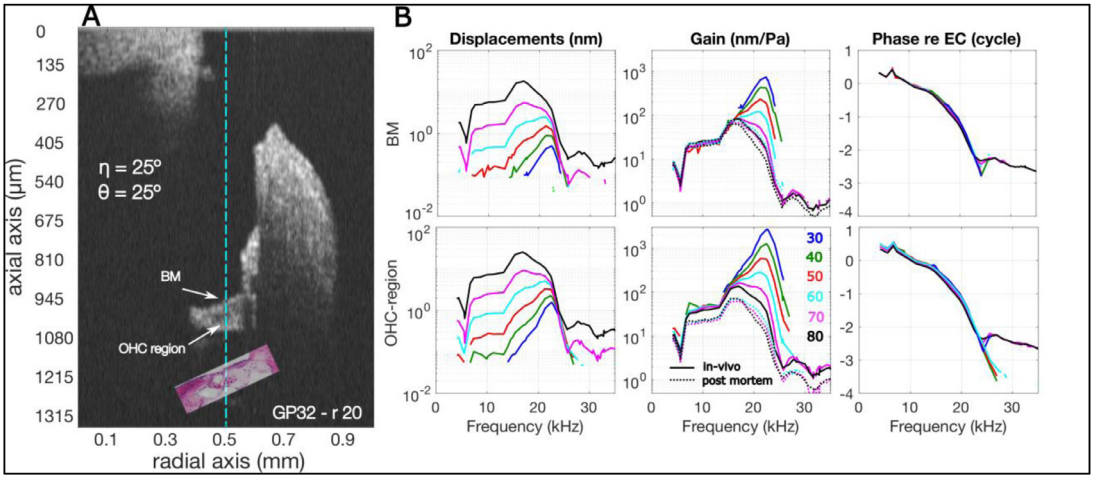

Fig. 3. (A) *B*-scan image in the base of the cochlea in guinea pig. The angle formed between the OCT beam and the axis of the OHCs was ~ 25°. (B) The motion responses of the BM (top row) and a layer ~75 μm deeper (bottom row). Solid lines = *in-vivo* motion responses. Dashed lines = post-mortem motion responses.

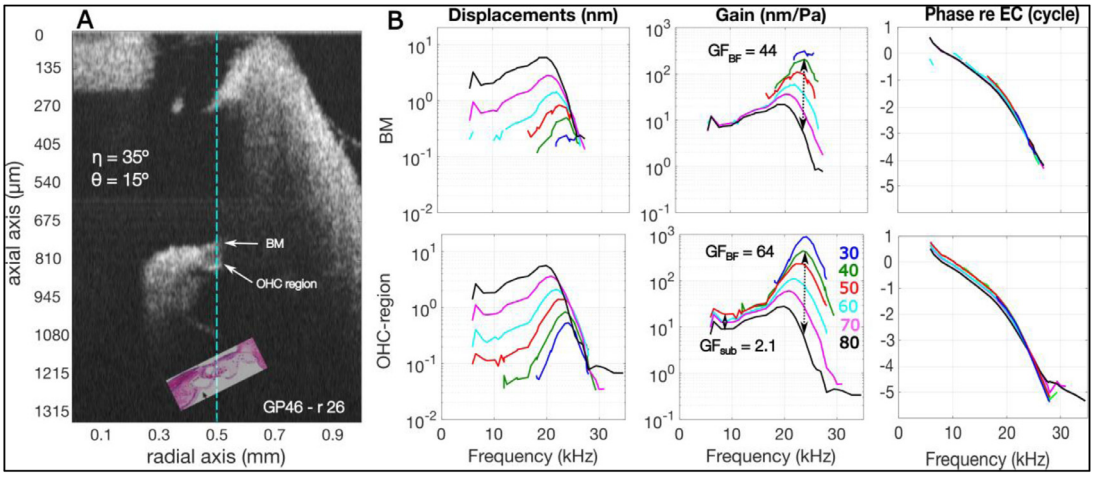

Fig. 4. (A) *B*-scan image in the base of the cochlea in guinea pig. The angle formed between the OCT beam and the axis of the OHCs was ~ 15°. (B) The motion responses of the BM (top row) and a layer ~90 μm deeper (bottom row). Sub-BF nonlinearity was observed in the OHC-region motions.

Table 1
40 dB SPL motion gains at the BF (nm/Pa) and motion gain factors for the BM and OHC region responses to multi-tone stimuli at a sub-BF frequency (GF_{sub}) and at the BF (GF_{BF}) in eight guinea pig cochleae. GF_{sub} & GF_{BF} were defined as the ratio of the 40 dB SPL motion gain (nm/Pa) to the 80 dB SPL motion gain (nm/Pa). GF_{BF} was calculated using the BF found at 40 dB SPL. GF_{sub} was calculated for a single sub-BF frequency in the range from 9 to 11 kHz. In the results with * 40 dB SPL motions were in the noise in the 9–11 kHz range, thus GF_{sub} was calculated from 50 to 80 dB SPL in these cases. This also could limit the ability to determine Q_{10dB} and in those cases those entries are left blank. **Two values are shown; for the larger value (2.7) the four cases that were essentially linear sub-BF were excluded from the average. When the BM angle relative to the horizontal line (η) is greater than 35°, the angle formed between the axis of the OHCs and the OCT beam (θ) will be less than ~15°.

GP # - run #	**40 dB SPL gain at BF (nm/Pa)**		**GF_{BF}**		**GF_{sub}**		**Q_{10}**		η
	BM	**OHC-region**	**BM**	**OHC-region**	**BM**	**OHC-region**	**BM**	**OHC-region**	
GP 32 – r 22	523	915	25	38.5	0.9	2	3.4	3.9	25°
GP 35 – r 38	224	450	17	31	1	2.7	2.8	3	50°
GP 42 – r 18	191	219	17	18	1.1	4.2	5.1	5.1	35°
GP 46 – r 26	206	445	44	64	1	2.1	3.3	3.7	35°
GP 26 – r 24	242	889	27	50	1.1*	1.1*	3.7	3.9	30°
GP 29 – r 19	306	904	20	60	1*	1*	-	4.7	35°
GP 34 – r 30	148	313	7	11	1*	1.1*	-	3.3	40°
GP 45 – r 13	100	185	13	15	1*	0.9*	-	3	30°
Average ($N = 8$)	243	540	21	36	1	2.7, 1.9**	3.7	3.8	
Standard deviation	129	315	11	20	0.06	1.1	0.9	0.8	

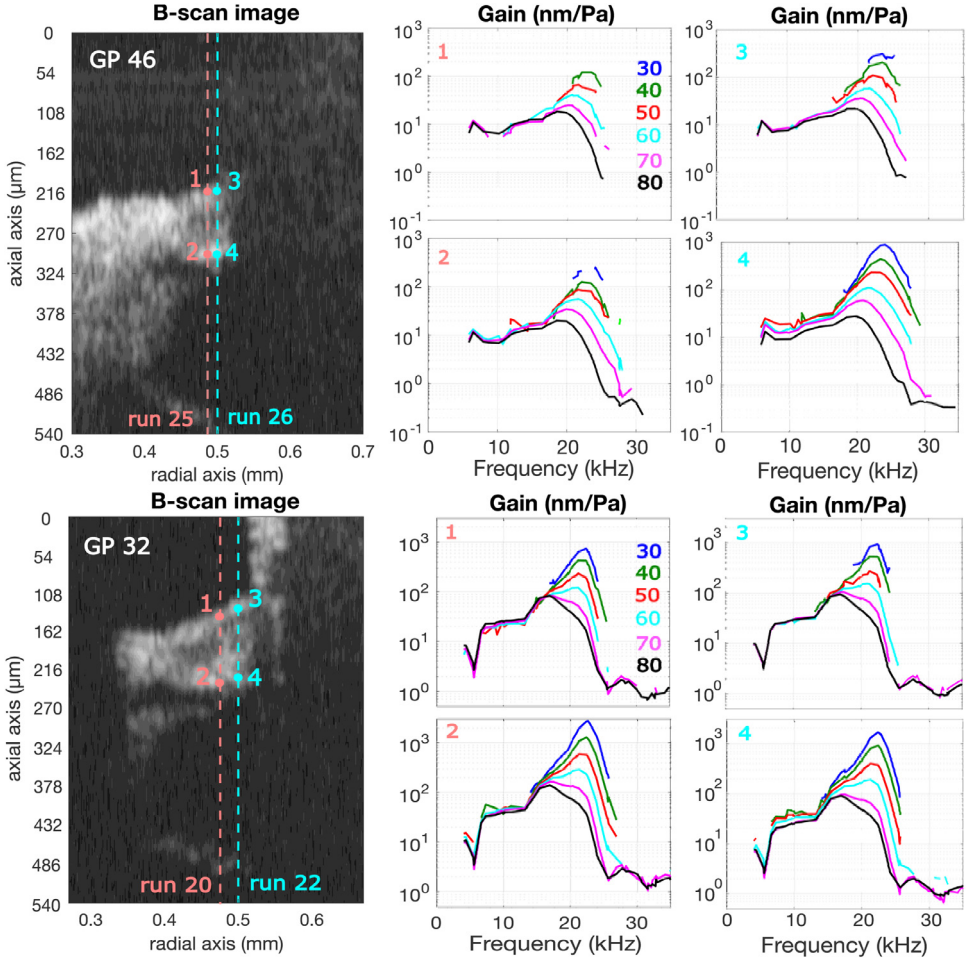

Fig. 5. Comparison of the amplitude of the intracochlear motion responses to multi-tone stimuli at two radial locations in two guinea pig cochleae. The degree of sub-BF nonlinearity within the OC varied laterally. The vertical (axial) resolution was ~2.7 μm per pixel and the *B*-scans axial axis is labeled in μm units.

location 1. Comparing the motions within the OC, the vibration at position 4 was 2 to 3 times larger than at location 2. Sub-BF nonlinearity was observed in the OC motion responses at the more lateral location 4, but not at position 2. In GP 32, the BM motion was slightly larger at the more lateral location (3 versus 1). However, the intra-OC motions at the more lateral location 4 were slightly smaller than at location 2. A small degree of OHC-region sub-BF nonlinearity was observed at the more lateral location 4, but not at location 2. In four of the eight displacement experiments, although we explored the radial space to the degree possible given the anatomical constraints, sub-BF nonlinearity was not detected.

3.2. Motion responses in gerbil

Fig. 6 shows the intracochlear motions in response to multi-tone stimuli in the base in gerbil. These data were published in Fallah et al. (2019) and replotted here to compare with the guinea pig results. In gerbil, the OCT beam was aimed to the OCC through the intact RW membrane. In the BF band, a similar nonlinear pattern was observed in gerbil and guinea pig: a large nonlinear peak in the BM motion. In recordings where the OCT beam was directed to the OHC region, the OHC-region motion was tuned to approximately the same BF as the BM motion. The phase of the motion relative to EC pressure accumulated through several cycles, indicating cochlear traveling wave delay. Sub-BF, nonlinearity was observed in the OHC region and the BM region was linear. We observed OHC-region sub-BF nonlinearity in all experiments in healthy gerbil cochleae - six from Fallah et al. (2019); and thirteen from Strimbu et al. (2020). The 40 dB SPL BM and OHC-region gains (nm/Pa), and the 40–80 dB SPL gain factors GF_{BF} and GF_{sub} for eight gerbil cochleae, selected based on good SNR, are tabulated in Table 2. The 40 dB SPL motion and GF_{BF} were substantially greater in the OHC region than at the BM. The $Q_{10\ dB}$ values spanned from 3.5 to 5.7 and were generally similar in the two regions (Table 2); a statistical comparison is in Fig. 9.

3.3. Comparisons between guinea pig and gerbil

3.3.1. Hyper-compression in motion

BF-band hyper-compression in the OHC-region motion: Fig. 7 A-B show the BM (dotted lines) and the OHC-region (solid lines) motion gains in one guinea pig and one gerbil cochlea. In guinea pig the OHC region gain is larger than the BM at all SPLs, whereas in gerbil at 70 and 80 dB SPL at many frequencies the BM moves more than the OHC region. This is related to "hyper-compression" whereby responses actually diminish as SPL is raised (Fallah et al., 2019; Cooper et al., 2018). Hyper-compression is easier to discern in the lower panels C-D where the OHC-region displacement, in nanometers, is plotted rather than the gain. In gerbil (panel *D*) strong hyper-compression is observed at 70–80 dB SPL, where the curves undercut the lower SPL curves. This degree of hyper-compression was a common finding in gerbil. In guinea pig an only a small degree of hyper-compression appears, at 80 dB SPL, where

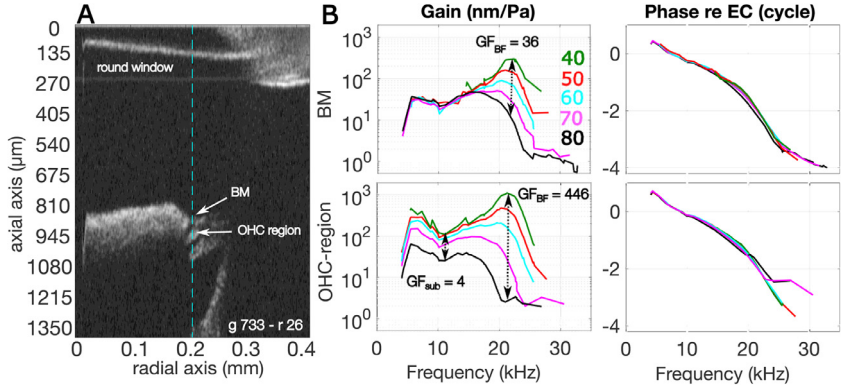

Fig. 6. (A) *B*-scan image from the organ of Corti in the base of the cochlea in gerbil. The OCT beam was directed through the OHCs. (B) The motion responses of the BM (top row) and a layer ~50 μm deeper (OHC-region, bottom row). Sub-BF nonlinearity was observed in the OHC-region motions.

Table 2
40 dB SPL motion gains at the BF (nm/Pa), motion gain factors and $Q_{10\ dB}$ values for the intracochlear motion responses to multi-tone stimuli at a sub-BF frequency (GF_{sub}) and in the BF (GF_{BF}) in eight gerbil cochleae. The parameter values were calculated as in Table 1.

	40 dB SPL gain at BF (nm/Pa)		GF_{BF}		GF_{sub}		Q_{10}	
g # - run #	**BM**	**OHC-region**	**BM**	**OHC-region**	**BM**	**OHC-region**	**BM**	**OHC-region**
g 794 – r 16	235	1350	11.5	208	1.1	4.6	4.8	5.3
g 789 – r 06	139	1058	21	350	0.9	4.5	-	4.6
g 786 – r 12	276	1049	72	216	1	6.2	5.5	4.9
g 733 – r26	302	1115	36	446	1	4	3.5	3.6
g 784 – r 09	234	801	38	368	0.8	4.5	5.4	4.4
g 781 – r 06	251	881	27	150	1	4.6	5.2	5.7
g 785 – r 09	185	1230	24	405	1	3.7	-	5.2
g 783 – r 12	184	877	24	467	1.1	4.8	5.6	4.4
Average ($N = 8$)	226	1045	32	326	1	4.5	5	4.8
Standard deviation	53	188	18	119	0.08	0.8	0.7	0.7

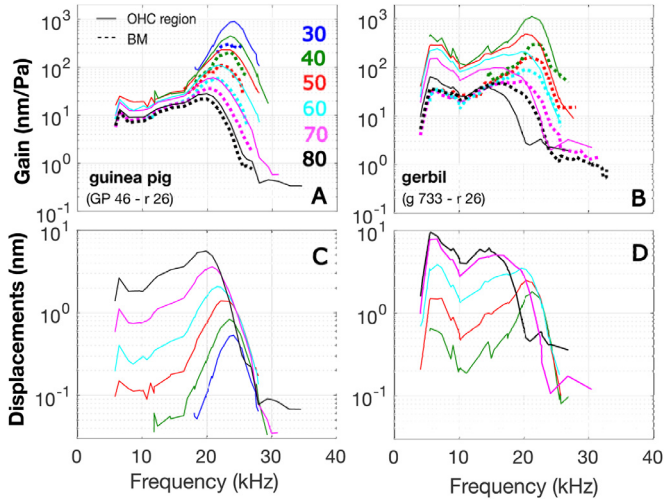

Fig. 7. Hyper-compression: top panels A,B: The gain amplitude of the BM (dotted lines) and OHC-region (solid lines) motion gain responses are plotted together for a guinea pig cochlea (GP 46) and gerbil cochlea (g733). Bottom panels C,D. OHC region motions, unnormalized.

in panel *C* the 80 dB curve undercuts the 30–70 dB curves starting at ~ 22 kHz.

3.3.2. LCM results

The amplitude, gain (LCM re EC pressure, mV/Pa), and phase of the LCM responses to multi-tone stimuli in two guinea pigs and one gerbil are shown in Fig. 8. (The gerbil LCM data were first published in Fallah et al. (2019) and are included here for comparison. LCM measurements in gerbil were made through a cochleostomy as in guinea pig.) In the guinea pig experiments, the voltage electrode was inserted into the first turn scala tympani, and advanced a distance of ~ 0.5–0.7 mm from the bony wall, to a position close to the BM. When the electrode was in position, the LCM phase relative to the EC pressure went through several cycles with characteristic traveling wave delay, which assured that the OHCs contributing to the responses were localized to a fairly narrow longitudinal region of the cochlea. In both species, nonlinear growth in both the BF and the sub-BF bands was observed. In guinea pig the robust sub-BF nonlinearity in LCM is in contrast to the weak sub-BF nonlinearity observed in OHC-region motion responses. (Fig. S2 and Fig. 8 row 3 show these sets of results for the same animal.) In both species, nonlinearity was much larger in the BF band, where LCM responses showed compressive nonlinearity except at the lowest SPLs in both species. The LCM responses to single tone stimuli were also measured and examples from guinea pig and gerbil are in Fig. 8, and show that the multi-tone produces substantially more sub-BF nonlinearity. This is reasonable because the overall stimulus magnitude is greater (Fallah et al., 2019; Versteegh and van der Heijden, 2012).

LCM gain factors (GF), defined as the ratio of the LCM gain (mV/Pa) from low (20 dB SPL) to high (70 dB SPL) stimulus amplitudes, are tabulated at the BF and sub-BF in Table 3. Because at high SPL the LCM responses could become non-local (no longer showing traveling wave phase accumulation) we chose to use a 20–70 dB SPL range to calculate LCM GF, rather than the 40–80 dB SPL range used for motion. The multi-tone responses are used in Table 3. Table 3 shows the LCM gain factors at f ~ 7–9 kHz (GF_{sub}) and at the BF (GF_{BF}) for eight guinea pig and seven gerbil cochleae. Both at the BF and sub-BF, the gain factors in guinea pig LCM responses were less than the gain factors in gerbil. The LCM in all

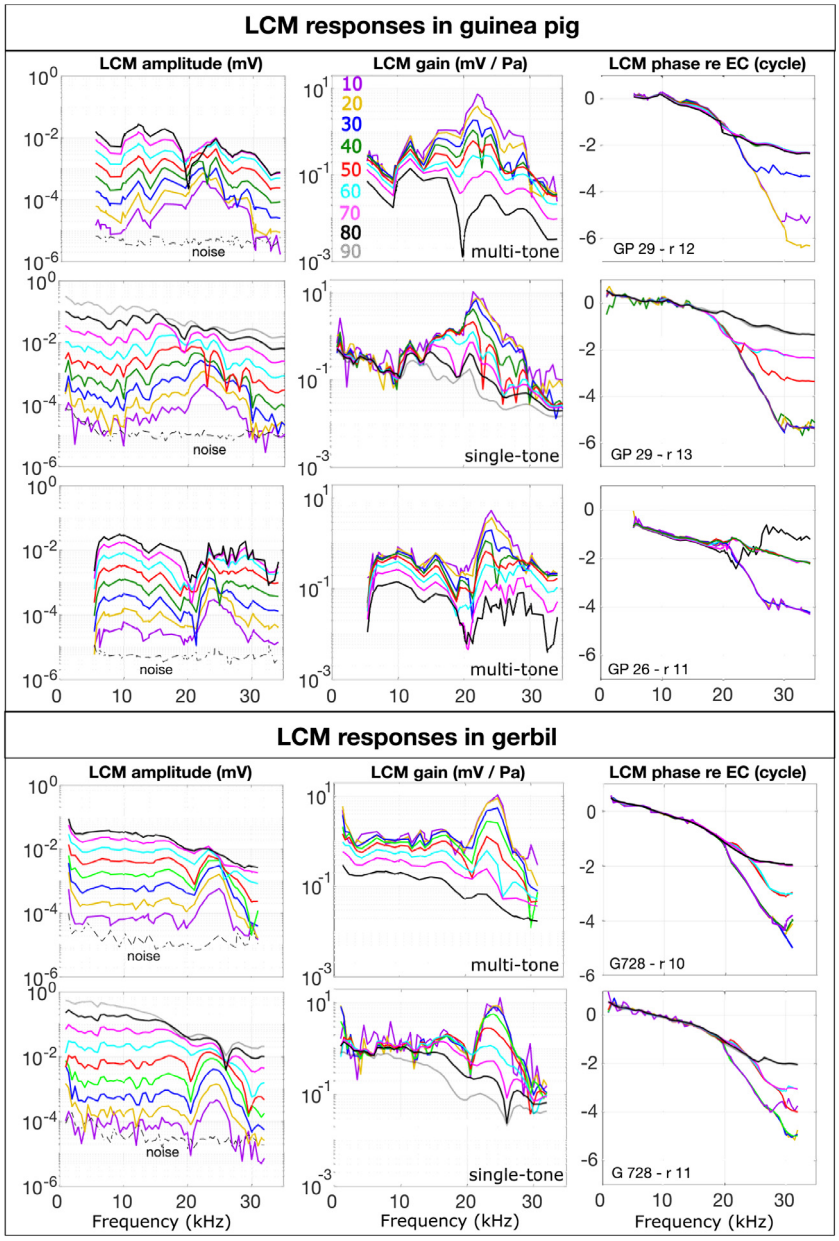

Fig. 8. Amplitude (left column), gain (middle column) and phase (right column) of the local cochlear microphonic (LCM) responses to multi-tone and single tone stimuli measured in the first turn in guinea pig (row 1–3) and in gerbil (row 4 & 5).

Table 3
Gain factors for the local cochlear microphonic (LCM) responses to multi-tone stimuli at a sub-BF frequency (GF_{sub}) and at the BF (GF_{BF}) in eight guinea pig and seven gerbil cochleae. GF_{sub} & GF_{BF} were defined as the ratio of the 20 dB SPL LCM gain (mV/Pa) to the 70 dB SPL LCM gain (mV/Pa). GF_{sub} was calculated at a sub-BF frequency in the range from ~7 to 9 kHz. For the * values, the averages were calculated using just the experiments with peak LCM gain at least 7mV/Pa, as explained in the text. Averaged LCM GF_{sub} in guinea pig is significantly smaller than the averaged LCM GF_{sub} in gerbil ($p < 0.001$, one-tailed unpaired t test with Welch's correction.

Guinea Pig			**Gerbil**		
GP # - run #	**GF_{sub}**	**GF_{BF}**	**g # - run #**	**GF_{sub}**	**GF_{BF}**
GP 29 – r 12	2.8*	44*	**g 690 – r 29**	3.5*	68*
GP 26 – r 11	2.3*	37*	**g 694 – r 10**	4.2	29
GP 6 – r 20	2.2	13	**g 697 – r 13**	3.2	41
GP 34 – r 23	2.1	11	**g 712 – r 18**	3.5*	147*
GP 23 – r 52	2.0	6	**g 720 – r 11**	2.4	6
GP 21 – r 33	2.8	11	**g 728 – r 10**	3.9*	87*
GP 18 – r 16	1.7	17	**g 730 – r 10**	3.4*	30*
GP 35 – r 31	2.9	14			
Average (N = 8)	2.3 (2.5*)	19 (40.5*)	**Average (N = 7)**	3.4 (3.6*)	58 (83*)
Standard deviation	0.4	13	**Standard deviation**	0.6	47

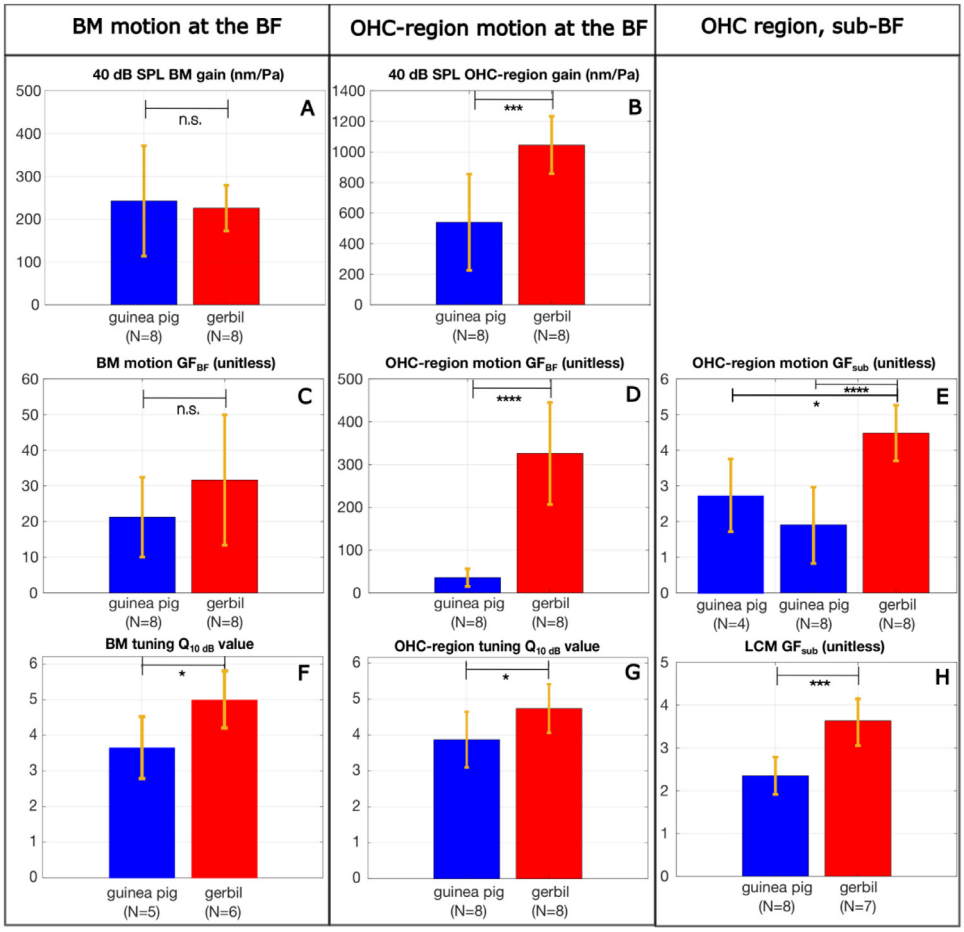

Fig. 9. (A) Averaged 40 dB SPL BM motion gain (nm/Pa) from eight preparations. (B) Averaged 40 dB SPL OHC-region motion gain (nm/Pa) from eight preparations. (C–E) Averaged BM and OHC-region motion gain factors in guinea pig (blue bars) and in gerbil (red bars) cochleae ± s.d. (yellow lines). (C) BM motion gain factor at the BF (GF_{BF}) from eight preparations. (D) OHC-region motion GF_{BF} from eight preparations. (E) OHC-region motion gain factor at a frequency sub-BF (GF_{sub}) from four and eight preparations. (F) Q_{10dB} values of the 40 dB SPL BM motion gains from five guinea pig and seven gerbil cochleae. (G) Q_{10dB} values of the 40 dB SPL OHC-region motion gains from eight preparations. (H) LCM GF_{sub} from eight guinea pig and seven gerbil cochleae. Data are means ± s.d. from Tables 1–3. $^{****}P < 0.0001$; $^{***}P < 0.001$; $^{*}P < 0.05$; n.s., not significant; one-tailed unpaired t test with Welch's correction.

eight guinea pig cochleae showed a BF peak, and traveling wave delay through several cycles, which means the responses were due to a reasonably localized population of OHCs. The LCM gain and gain factors in both species varied over a large range. Only four of the gerbil data sets and two of the guinea pig data sets attained LCM gain values greater than 7 mV/Pa. The wide range in LCM values is likely in part due to variation in placing the electrode in a "good" position close to the BM, because the placement was done somewhat blindly and one hesitates to get too close and damage the OCC. Thus, in Table 3, we also include the average when only the featured, "best", LCM data (LCM gain values greater than 7 mV/Pa) are included (entries with *). This influenced the GF_{BF} average considerably but had little effect on the GF_{sub} average, which was within a standard deviation of the mean of all eight. Even with the limited data sets, only comparing the "best" guinea pig and gerbil preparations, GF_{BF} and GF_{sub} for guinea pig remained lower than for gerbil. Two additional LCM measurements are included in the supplemental information, one for each species (Fig. S3), to show that the data sets with lower LCM voltage value were tuned, nonlinear and possessed traveling wave phase accumulation, and are reasonable to include in the tabulated data, with the caveat that higher voltages might have been attained in these preparations with more optimal electrode placement.

3.3.3. Grouped data comparison between guinea pig and gerbil

In the bar graphs of Fig. 9 the gerbil and guinea pig cochlear responses are compared in grouped data.

40 dB SPL motion gain at the BF: We observed a substantial overlap between the 40 dB SPL BM motion gain at the BF in the two species (BM motion $243 \pm 129 \frac{nm}{Pa}$ ($N = 8$) in guinea pig; $226 \pm 53 \frac{nm}{Pa}$ ($N = 8$) in gerbil, Fig. 9A). In contrast to the BM, in the OHC-region, we observed a significantly smaller 40 dB SPL motion gain at the BF in guinea pig compared to gerbil (OHC-region motion $540 \pm 315 \frac{nm}{Pa}$ ($N = 8$) in guinea pig; $1045 \pm 188 \frac{nm}{Pa}$ ($N = 8$) in gerbil, Fig. 9B).

Gain factors, BF band: In harmony with our gain findings at the BF, we observed a substantial overlap between the BM motion GF_{BF} in the two species ($21 \pm 11 (N = 8)$ in guinea pig; $32 \pm 18 (N = 8)$ in gerbil, Fig. 9C). In contrast, in the OHC-region motion we found a significantly smaller degree of compressive nonlinearity in guinea pig compared to gerbil ($GF_{BF} = 36 \pm 21 (N = 8)$ in guinea pig; $326 \pm 119 (N = 8)$ in gerbil, Fig. 9D). A lower degree of nonlinearity in the BF LCM responses was observed in guinea pig versus gerbil (LCM GF_{BF} = 40.5 for guinea pig vs 83 for gerbil, Table 3, using the reduced * data sets). The * data sets in guinea pig were too sparce for a statistical comparison and we do not include a bar graph with BF LCM gain.

Gain factors, sub-BF band: Sub-BF, the BM motion was linear in both species. Nonlinearity was observed in the OHC region but the degree of nonlinearity was less in guinea pig than in gerbil, and as noted above it was detected only in four of eight healthy guinea pig cochleae compared to every gerbil cochlea (OHC-region motion $GF_{sub} = 2.7 \pm 1.1$ (N = 4) in guinea pig; 4.5 ± 0.8 (N = 8) in gerbil, Fig. 9E.) The OHC-region motion GF_{sub} difference between guinea pig and gerbil was statistically significant, even when the four guinea pigs that did not display obvious nonlinearity were excluded. The degree of sub-BF nonlinearity in the LCM responses was also significantly lower in guinea pig versus gerbil (LCM $GF_{sub} = 2.3 \pm 0.4$ (N = 8) in guinea pig; 3.4 ± 0.6 (N = 6) in gerbil, Fig. 9H).

Sharpness of tuning (Q_{10dB} value): Within each species, there was substantial overlap in Q_{10dB} values between the BM and the OHC-region motions. Comparing the Q_{10dB} values across the species, we observed a sharper tuning in the intracochlear motions in gerbil compared to guinea pig (BM motion: $Q_{10dB} = 3.7 \pm 0.9$ (N = 5) in guinea pig; 5 ± 0.7 (N = 7) in gerbil. OHC-region motion: $Q_{10dB} = 3.8 \pm 0.8$ (N = 8) in guinea pig; 4.8 ± 0.7 (N = 8) in gerbil, Fig. 9 F and G).

4. Discussion

Our intracochlear motion and LCM responses in guinea pig are consistent with previous basal measurements in healthy guinea pig cochleae. Nuttall et al. (2018) observed a BM motion GF_{BF}~ 8 from 40 to 80 dB SPL and a LCM GF_{BF}~ 35 from 20 to 70 dB SPL in response to three-tone stimuli. Chen et al. (2011) observed a BM motion GF_{BF}~ 7.5 and RL motion GF_{BF}~ 12.5 from 40 to 80 dB SPL in response to single tones. The 40 dB sensitivities (gains) are within a factor of ~6 of those reported in these previous studies, a reasonable consistency considering the methodological differences in the different studies. The small degree of hyper-compression in guinea pig is consistent with the RL motion data in guinea pig (Chen et al., 2011). Our experiments went beyond the previous in reporting displacement from OHC and BM regions simultaneously, and in exploring radial and directional variations in displacement.

The cochlea possesses a mechanism for tuning amplification to achieve sharp frequency selectivity. OHC electromotility is known as an essential component of cochlear tuning. What we know is that (1) intracellular voltage changes drive the OHCs to exert a mechanical force. (2) Intracellular voltage and thus mechanical force are nonlinear across stimulus amplitudes. (3) The OHC voltage-driven mechanical force is in the direction of the axis of the OHCs (Frank et al., 1999). (4) The OHCs are embedded in the organ of Corti, and the orientation of the OHCs and supporting cells relative to the BM (Yoon et al., 2011), the fluid gaps inside the cochlea (Karavitaki and Mountain, 2007; Cooper et al.,2018), and the TM attachment to the OHC hair bundle (Lagarde et al., 2008), all create a suitable platform to obtain cochlear tuning. Still, there is much to be learned about how cochlear tuning is produced.

In a previous study in the base of the cochlea in gerbil (Fallah et al., 2019) we observed a different pattern of nonlinearity in the displacements of the BM versus the OHC-region. In particular, robust *sub-BF* nonlinearity was observed in the OHC-region motions. Robust sub-BF nonlinearity was also seen in the LCM responses and we concluded that the sub-BF OHC-region displacements were primarily due to wideband OHC electromotility. The sub-BF OHC-based activity did not transfer to the BM in the cochlear base. The present study compares these previous findings in gerbil to new findings in guinea pig.

In the BF band, BM motions were similar in the two species. In contrast, the OHC-region gain at 40 dB SPL was twice as large in gerbil than guinea pig, and the motion GF_{BF} in gerbil was on average nine times larger than in guinea pig. A higher GF_{BF} in the LCM responses was also observed in gerbil versus guinea pig. In the sub-BF band, BM motion was linear in both species, and nonlinearity was observed in the OHC region in both species. However, the nonlinear sub-BF OHC-region motion was weaker in guinea pig and was detected only in four of eight healthy guinea pig cochleae, whereas in gerbil we robustly observed sub-BF nonlinearity in the OHC-region. The large OHC-region nonlinearity in gerbil is partly a product of the phenomenon of hyper-compression, in which the size of responses decreases with increases in sound pressure level. Hyper-compression was barely present in our observations in guinea pig. Sub-BF nonlinearity in the LCM responses was robustly detected in both species, and slightly smaller (by a factor of ~ 0.7) in guinea pig.

We probed the motion in guinea pig by considering angle of approach and radial location. In guinea pig, measurements were made through a cochleostomy, located apically of the round window. The OCT beam was directed to the OCC in the transverse plane, without a significant longitudinal component. Because of the small opening there was not a possibility for changing the viewing angle in an individual preparation, but due to variations in the placement of the cochleostomy, the angle varied in different experiments (Fig. 2). We predicted that sub-BF nonlinearity would be present when the viewing angle was more in line with the OHC axis. However, this expectation was not borne out in the measurements (Table 1). In gerbil, we approached the ~ 22 kHz BF band by aiming the OCT beam apically through the intact round window membrane, and thus the direction of the OCT beam was not completely in the transverse plane of the OCC, and had a substantial longitudinal component. In other cases, we made measurements in the ~ 30–40 kHz band, where the optical axis was approximately in the transverse plane. Sub-BF nonlinearity in the OHC region was robustly present for both these viewing angles in gerbil. The fact that we observed nonlinear sub-BF OHC motion from different directions in gerbil is consistent with the study by Cooper et al. (2018). They argued that the OHC-region motion in gerbil is elliptical, with a substantial longitudinal component.

The variation with radial location (Fig. 5) showed that sub-BF nonlinearity in or close to the OHC region could emerge with a small variation in radial location, along with an increase in the size of that motion (GP46). In GP32 sub-BF nonlinearity in the apparent OHC-region also emerged at the more lateral location, along with (unexpectedly) a decrease in the size of the motion. In both these examples, the region of sub-BF nonlinearity was narrow, and in other guinea pig cochleae, radial variations - probed to the extent possible, given anatomical constraint - did not reveal sub-BF nonlinearity. In gerbil, a robust and readily detectable "hot spot" region is present where motion is largest, and sub-BF nonlinearity is largest (Fallah et al., 2019; Cooper et al., 2018; Strimbu et al., 2020). In summary, in spite of our efforts with angle and radial variations, the detection of robust sub-BF nonlinearity was elusive in the guinea pig. Nevertheless, as tabulated in Table 1, at the BF the OHC region moved more than the BM in the healthy guinea pig cochlea.

The differences observed in intra-OCC motion patterns - consistent and vigorous sub-BF nonlinearity in the OHC region of gerbils, and weaker, inconsistent sub-BF nonlinearity in guinea pig, coupled to lower OHC-region nonlinearity in the BF band - must be rooted in the differences in the anatomy and physiology of the cochlea of gerbils and guinea pigs. Gerbils are from the murid family of rodents, which includes rats and mice, and guinea pigs are a non-murid species (Reyes et al., 2000; Vater and Kossl, 2011). Gerbils are altricial animals whose ears develop substantially after birth (Arjmand et al., 1988) while guinea pigs are precocial with functional ears at birth. From the anatomical perspective, despite the fact that guinea pigs and gerbils have a similar hear-

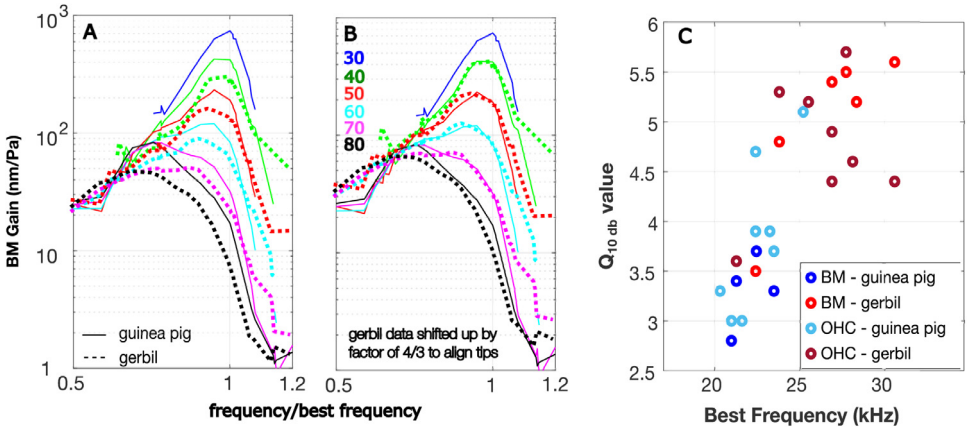

Fig. 10. (A) The BM motion gain responses in guinea pig (solid lines, GP32 r20, BF = 22.4 kHz) and in gerbil (dotted lines, g733 r26, BF = 22.4 kHz) are plotted together. The *x*-axis is normalized to the BF. (B) gerbil data was shifted vertically by a factor of 4/3 so that the 40 dB SPL peaks line up. (C) $Q_{10\ dB}$ values of the 40 dB SPL BM and OHC-region motion responses in guinea pig and gerbil. Within each species, positive correlations were observed between the intracochlear-motion $Q_{10\ dB}$ values and the BF ($r = 0.86$, $p < 05$ for the BM motions in both gerbil and guinea pig, $r = 0.78$, $p < 01$ for the OHC-region motion in guinea pig, $r = 0.26$, $p = 0.2$ for the OHC-region motion in gerbil). The BM-motion based BFs of the runs are as follows: GP32-r22 21.3 kHz; GP35-r38 21 kHz; GP42-r18 25.2 kHz; GP46-r26 23.5 kHz; GP26-r24 22.5 kHz; GP29-r19 21.9 kHz; GP34-r30 19.6 kHz; GP45-r13 21.6 kHz; g794-r16 23.8 kHz; g789-r6 28.1 kHz; g786-r12 27.7 kHz; g733-r26 22.4 kHz; g784-r9 26.9 kHz; g781-r6 28.4 kHz; g785-r9 25.5 kHz; g783-r12 30.6 kHz.

ing frequency range, the guinea pig cochlea has one turn more than the gerbil cochlea (Teudt and Richter, 2007, Edge et al., 1998, Fay, 1989) and the length of the BM is ~ 18 mm in guinea pig (Wada et al., 1998) versus ~11 mm in gerbil (Plassmann et al., 1987). Thus, guinea pigs devote more OHCs and a greater length of cochlear processing to a given frequency range.

The longitudinal variation in BM properties from the base to the apex is not the same between guinea pigs and gerbils. In guinea pig, the frequency map seems to rely more on macro-scale anatomical and structural variations: the decrease of the BM stiffness is in line with a mostly steady increase in the BM width and decrease in the BM thickness from the base to the apex (Fernández, 1952; Wada et al., 1998). In gerbil, the BM width has a sharp increase in the very base beyond which it barely changes. The BM thickness shows little variation in the base followed by a sharp increase and then an unchanging thickness (Plassmann et al., 1987). Nevertheless, these BM variations in gerbil result in a consistent decrease in the BM stiffness from the base to the apex (Emadi et al., 2004; Naidu and Mountain, 1998; Richter et al., 2007). The unusual arch shape of the BM in gerbil also differentiates this animal from guinea pig and other species, and has been proposed to be fundamental to determining the stiffness (Kapuria et al., 2011, 2017).

In gerbil, a phase shift of LCM versus BM motion has been observed at a frequency below the BF peak (Dong and Olson, 2013). The shift, probably sourced in the mechanics of the stereocilia and tectorial membrane, would serve to uncouple sub-BF electromotility from the mechanism that amplifies the BM traveling wave (Dong and Olson, 2013; Nankali et al., 2020). It is not clear if such a mechanism exists in guinea pig (Fridberger et al., 2004), but based on the smaller size of the sub-BF nonlinearity in guinea pig, there might be less need to uncouple sub-BF electromotility from the BM in this species. To explore subtle phase differences between voltage and BM motion and pursue this question in guinea pig requires simultaneous measurements; these experiments are in the planning stages. While the significance of sub-BF nonlinearity to hearing is not obvious, the way the system manages to exclude it from basal cochlear BM responses is an interesting and illuminating aspect of cochlear amplification.

In spite of these observed and formerly documented differences, ultimately the BM response sizes and degrees of nonlinearity in the two species were very similar when observed at the same BF (Fig. 10). Fig. 10A shows the motion gains and in Fig. 10B the gerbil data has been shifted vertically by a factor of 4/3 so that the 40 dB SPL data line up in the peak. In this comparison, the guinea pig motion was slightly larger than gerbil, but as tabulated above, there is much overlap between the two species in this metric. Fig. 10 illustrates how nearly indistinguishable the amplitude responses of the two species is at the level of BM motion. The comparison in Fig. 10 showed that the Q_{10dB} value was slightly higher in gerbil than guinea pig. One explanation for the larger Q_{10dB} in gerbil could be because the gerbil motion measurements were obtained from locations with slightly higher BF. We observed a positive correlation between Q_{10dB} values and the BF within each species (Fig. 10C), consistent with previous measurements from auditory nerve fibers in gerbil (van der Heijden and Joris, 2003; Ohlemiller and Echteler,1990). When comparing the same BF between species the Q_{10dB} of single nerve fibers showed no substantial differences in the high frequency band (Ohlemiller and Echteler,1990; Robertson and Manley, 1974).

A final note relates to the post-mortem changes that were observed. At the BM, in virtually all mammals studied, including the gerbil and guinea pig responses reported here, the sub-BF band is linear and "passive" with little or no change post-mortem. Sub-BF intra-OCC nonlinearity is strong in gerbil, and disappears post-mortem (Cooper et al., 2018; Strimbu et al., 2020). In guinea pig, within the OCC we observed only weak sub-BF nonlinearity. It was therefore a surprise to observe a significant reduction in linear sub-BF motion within the OC post-mortem (Fig. 3 and supplementary Fig. S2). If this "active" (physiologicially vulnerable) motion was due to electromotility, it would be expected to be nonlinear, based on the observed nonlinear sub-BF LCM. Therefore, the post-mortem condition apparently caused a change that was not directly related to electromotility. The change might be due to a static position change when EP dropped post-mortem, leading to a reduced sub-BF motion. This post-mortem observation relates to findings of static position changes in *in-vitro* studies in guinea pig (Jacob et al., 2011) as well as operating point shifts during recovery post-furosemide in gerbil (Wang et al., 2018, 2019; Strimbu et al., 2020), theories of automatic gain control (Cooper et al., 2018) and consideration of mode shifts, for example as presented in a recent review (Guinan, 2020).

5. Conclusion

In this study, we measured the intra-OCC motions and the electrophysiological LCM responses in the base of the cochlea in guinea pig. Comparing to our previous study under the same experimental conditions in gerbil, we observed a lower degree of nonlinearity in guinea pig than gerbil and a qualitative difference in sub-BF motions. These physiological differences, and the macro-scale anatomical differences between the two species, suggest that although basic similarities are present, on a more subtle level these animals may have devised different ways to produce the cochlear frequency map and sharp frequency tuning.

6. Author contributions

E. F. performed the OCT experiments in guinea pig, and the LCM experiments in guinea pig and gerbil, analyzed data and drafted the paper. C. E. S. performed the OCT experiments in gerbil and analyzed data. E. S. O. supervised the experiments and contributed to the writing of the paper.

Acknowledgments

This work was funded by NIH grant R01-DC015362 and the Emil Capita Foundation.

Supplementary materials

Supplementary material associated with this article can be found, in the online version, at doi:10.1016/j.heares.2021.108234.

References

Arjmand, E., Harris, D., Dallos, P., 1988. Developmental changes in frequency mapping of the gerbil cochlea: comparison of two cochlear locations. Hear. Res. 32 (1), 93–96.
Chen, F., Zha, D., Fridberger, A., Zheng, J., Choudhury, N., Jacques, S.L., Nuttall, A.L., 2011. A differentially amplified motion in the ear for near-threshold sound detection. Nat. Neurosci. 14 (6), 770.
Cooper, N.P., Rhode, W.S., 1992. Basilar membrane mechanics in the hook region of cat and guinea-pig cochleae: sharp tuning and nonlinearity in the absence of baseline position shifts. Hear. Res. 63 (1-2), 163–190.
Cooper, N.P., Vavakou, A., van der Heijden, M., 2018. Vibration hotspots reveal longitudinal funneling of sound-evoked motion in the mammalian cochlea. Nat. Commun. 9 (1), 1–12.
De Boer, E., Nuttall, A.L., 1997. The mechanical waveform of the basilar membrane. I. Frequency modulations ("glides") in impulse responses and cross-correlation functions. J. Acoust. Soc. Am. 101 (6), 3583–3592.
De Boer, E., Nuttall, A.L., 2000. The mechanical waveform of the basilar membrane. III. Intensity effects. J. Acoust. Soc. Am. 107 (3), 1497–1507.
Dong, W., Olson, E.S., 2013. Detection of cochlear amplification and its activation. Biophys. J. 105 (4), 1067–1078.
Dong, W., Olson, E.S., 2016. Two-tone suppression of simultaneous electrical and mechanical responses in the cochlea. Biophys. J. 111 (8), 1805–1815.
Edge, R.M., Evans, B.N., Pearce, M., Richter, C.P., Hu, X., Dallos, P., 1998. Morphology of the unfixed cochlea. Hear. Res. 124 (1-2), 1–16.
Emadi, G., Richter, C.P., Dallos, P., 2004. Stiffness of the gerbil basilar membrane: radial and longitudinal variations. J. Neurophysiol. 91 (1), 474–488.
Eze, N., Olson, E.S., 2011. Basilar membrane velocity in a cochlea with a modified organ of Corti. Biophys. J. 100 (4), 858–867.
Fallah, E., Strimbu, C.E., Olson, E.S., 2019. Nonlinearity and amplification in cochlear responses to single and multi-tone stimuli. Hear. Res. 377, 271–281.
Fay, R.R., 1989. Hearing in Vertebrates: A Psychophysics Databook. Hearing in Vertebrates: A Psychophysics Databook. Hill-Fay Associates, Winnetka, Illinois.
Fernández, C., 1952. Dimensions of the cochlea (guinea pig). J. Acoust. Soc. Am. 24.5, 519–523.
Frank, G., Hemmert, W., Gummer, A.W., 1999. Limiting dynamics of high-frequency electromechanical transduction of outer hair cells. Proc. Natl. Acad. Sci. 96 (8), 4420–4425.
Fridberger, A., De Monvel, J.B., Zheng, J., Hu, N., Zou, Y., Ren, T., Nuttall, A., 2004. Organ of Corti potentials and the motion of the basilar membrane. J. Neurosci. 24 (45), 10057–10063.
Geisler, C.D., Yates, G.K., Patuzzi, R.B., Johnstone, B.M., 1990. Saturation of outer hair cell receptor currents causes two-tone suppression. Hear. Res. 44 (2-3), 241–256.
Greenwood, D.D., 1990. A cochlear frequency-position function for several species—29 years later. J. Acoust. Soc. Am. 87 (6), 2592–2605.
Guinan, J.J., 2020. The interplay of organ-of-corti vibrational modes, not tectorial-membrane resonance, sets outer-hair-cell stereocilia phase to produce cochlear amplification. Hear. Res., 108040.
Henson, M.M., 1973. Unusual nerve-fiber distribution in the cochlea of the bat Pteronotus p. Parnellii (Gray). J. Acoust. Soc. Am. 53 (6), 1739–1740.
Henson, M.M., Henson, O.W., Jenkins, D.B, 1977. The cochlea of the bat, Pteronotus p. Parnellii. J. Acoust. Soc. Am. 62 (S1) S85-S85.
Jacob, S., Pienkowski, M., Fridberger, A., 2011. The endocochlear potential alters cochlear micromechanics. Biophys. J. 100 (11), 2586–2594.
Kapuria, S., Steele, C.R., Puria, S., 2011. Mechanics of the unusual basilar membrane in gerbil. In: Proceedings of the AIP Conference Proceedings, 1403. American Institute of Physics, pp. 333–339 No. 1, pp..
Kapuria, S., Steele, C.R., Puria, S., 2017. Unraveling the mystery of hearing in gerbil and other rodents with an arch-beam model of the basilar membrane. Sci. Rep. 7 (1), 1–10.
Karavitaki, K.D., Mountain, D.C., 2007. Evidence for outer hair cell driven oscillatory fluid flow in the tunnel of Corti. Biophys. J. 92 (9), 3284–3293.
Lagarde, M.M.M., Drexl, M., Lukashkina, V.A., Lukashkin, A.N., Russell, I.J, 2008. Outer hair cell somatic, not hair bundle, motility is the basis of the cochlear amplifier. Nat. Neurosci. 11 (7), 746–748.
Lin, N.C., Hendon, C.P., Olson, E.S., 2017. Signal competition in optical coherence tomography and its relevance for cochlear vibrometry. J. Acoust. Soc. Am. 141 (1), 395–405.
Lin, N.C., Strimbu, C.E., Hendon, C.P., Olson, E.S., 2018. Adapting a commercial spectral domain optical coherence tomography system for time-locked displacement and physiological measurements. In: In AIP Conference Proceedings, 1965 (1). AIP Publishing LLC., p. 080004.
Manley, G.A., 2018. Travelling waves and tonotopicity in the inner ear: a historical and comparative perspective. J. Comp. Physiol. A 204 (9-10), 773–781.
Manley, G.A., 2010. An evolutionary perspective on middle ears. Hear. Res. 263 (1-2), 3–8.
Naidu, R.C., Mountain, D.C., 1998. Measurements of the stiffness map challenge a basic tenet of cochlear theories. Hear. Res. 124, 124–131.
Nankali, A., Wang, Y., Strimbu, C.E., Olson, E.S., Grosh, K., 2020. A role for tectorial membrane mechanics in activating the cochlear amplifier. Scientific Reports 10 (1), 1–15.
Narayan, S.S., Temchin, A.N., Recio, A., Ruggero, M.A., 1998. Frequency tuning of basilar membrane and auditory nerve fibers in the same cochleae. Science 282 (5395), 1882–1884.
Nuttall, A.L., Ricci, A.J., Burwood, G., Harte, J.M., Stenfelt, S., Cayé-Thomasen, P., Lunner, T., 2018. A mechanoelectrical mechanism for detection of sound envelopes in the hearing organ. Nat. Commun. 9 (1), 1–11.
Ohlemiller, K.K., Echteler, S.M., 1990. Functional correlates of characteristic frequency in single cochlear nerve fibers of the Mongolian gerbil. J. Comp. Physiol. A 167 (3), 329–338.
Olson, E.S., 2020. "Mechanics of the Cochlea: in Volume II, Audition of the Series "The Senses: A Comprehensive Reference, 2nd Edition Elsevier Publisher:.
Plassmann, W., Peetz, W., Schmidt, M., 1987. The cochlea in gerbilline rodents. Brain Behav. Evol. 30 (1-2), 82–102.
Rabbitt, R.D., 2020. The cochlear outer hair cell speed paradox. Proc. Natl. Acad. Sci. 117 (36), 21880–21888.
Raufer, S., Guinan, J.J., Nakajima, H.H., 2019. Cochlear partition anatomy and motion in humans differ from the classic view of mammals. Proc. Natl. Acad. Sci. 116 (28), 13977–13982.
Ren, T., 2002. Longitudinal pattern of basilar membrane vibration in the sensitive cochlea. Proc. Natl. Acad. Sci. 99 (26), 17101–17106.
Reyes, A., Gissi, C., Pesole, G., Catzeflis, F.M., Saccone, C., 2000. Where do rodents fit? Evidence from the complete mitochondrial genome of Sciurus vulgaris. Mol. Biol. Evol. 17 (6), 979–983.
Richter, C.P., Emadi, G., Getnick, G., Quesnel, A., Dallos, P., 2007. Tectorial membrane stiffness gradients. Biophys. J. 93 (6), 2265–2276.
Rhode, W.S., 1971. Observations of the vibration of the basilar membrane in squirrel monkeys using the Mössbauer technique. J. Acoust. Soc. Am. 49 (4B), 1218–1231.
Rhode, W.S., 2007. Basilar membrane mechanics in the 6–9 kHz region of sensitive chinchilla cochleae. J. Acoust. Soc. Am. 121 (5), 2792–2804.
Robertson, D., Manley, G.A., 1974. Manipulation of frequency analysis in the cochlear ganglion of the guinea pig. J. Comp. Physiol. 91 (4), 363–375.
Santos-Sacchi, J., 1993. Harmonics of outer hair cell motility. Biophys. J. 65 (5), 2217–2227.
Sellick, P.M., Yates, G.K., Patuzzi, R., 1983. The influence of Mossbauer source size and position on phase and amplitude measurements of the guinea pig basilar membrane. Hear. Res. 10 (1), 101–108.
Strimbu, C.E., Wang, Y., Olson, E.S., 2020. Manipulation of the endocochlear potential reveals two distinct types of cochlear nonlinearity. Biophys. J.
Teudt, I.U., Richter, C.P., 2007. The hemicochlea preparation of the guinea pig and other mammalian cochlea. J. Neurosci. Methods 162 (1-2), 187–197.
Thorne, M., Salt, A.N., DeMott, J.E., Henson, M.M., Henson, O.W., Gewalt, S.L, 1999. Cochlear fluid space dimensions for six species derived from reconstructions of three-dimensional magnetic resonance images. Laryngoscope 109 (10), 1661–1668.
Vater, M., Kössl, M., 2011. Comparative aspects of cochlear functional organization in mammals. Hear. Res. 273 (1-2), 89–99.
van der Heijden, M., Joris, P.X., 2003. Cochlear phase and amplitude retrieved from the auditory nerve at arbitrary frequencies. J. Neurosci. 23 (27), 9194–9198.

Versteegh, C.P., van der Heijden, M., 2012. Basilar membrane responses to tones and tone complexes: nonlinear effects of stimulus intensity. J. Assoc. Res. Otolaryngol. 13 (6), 785–798.
Wada, H., Sugawara, M., Kobayashi, T., Hozawa, K., Takasaka, T., 1998. Measurement of guinea pig basilar membrane using computer-aided three-dimensional reconstruction system. Hear. Res. 120 (1-2), 1–6.
Wang, Y., Fallah, E., Olson, E.S., 2018. Variations in OHC-generated voltage and DPOAEs with low EP. In: Proceedings of the AIP Conference (Vol. 1965, No. 1, p. 060006). AIP Publishing LLC.
Wang, Y., Fallah, E., Olson, E.S., 2019. Adaptation of cochlear amplification to low Endocochlear potential. Biophys. J. 116 (9), 1769–1786.
Yoon, Y.J., Steele, C.R., Puria, S., 2011. Feed-forward and feed-backward amplification model from cochlear cytoarchitecture: an interspecies comparison. Biophys. J. 100 (1), 1–10.